Over-the-air 26GHz Receiver Hardware-Software Evaluation towards Joint Communication and Radar Sensing

Sandra George[1], Padmanava Sen[1], Muhammad Umar[1], Maximilian Matthé[1], Jan Adler[1], Mehrab Ramzan[1], Corrado Carta[2]
[1]Barkhausen Institut, Dresden, Germany
[2]Technische Universität Berlin & IHP Microelectronics GmbH, Frankfurt an der Oder, Germany
{[1]sandra.george, [1]padmanava.sen [1]muhammad.umar, [1]maximilian.matthe, [1]jan.adler, [1]mehrab.ramzan,}@barkhauseninstitut.org
[2]carta@ihp-microelectronics.com

***Abstract*— Joint Communication and Sensing (JC&S) has been identified as a novel feature of future 6G systems to support innovative applications. This paper analyzes the performance of a unified communication and radar system while employing identical waveform and receiver for both functionalities. The paper also compares the effect of horn antennas and patch antennas for both radar and communication systems using a 26 GHz receiver developed in 22 nm Fully Depleted Silicon On Insulator (FDSOI) technology and packaged using wire bonding approach. An investigation of JC&S Key Performance Indicators (KPIs) in terms of interference, antenna isolation, receiver linearity requirements are also discussed. The hardware-software platform developed is scalable to different standards and custom hardware evaluation for JC&S use cases.**

***Keywords*— Antenna, receiver, Joint Communication and Sensing (JC&S), link-level evaluation**

I. Introduction

Joint Communication and Sensing (JC&S) is expected to be one of the key features of future 6G networks with possible sensing-as-a-service availability. An efficient realization of JC&S requires a co-optimized solution in terms of waveforms, antennas and radio frequency (RF) front-end in a co-design approach. Reconfigurable hardware is expected to play an important role in the integration of this technology with future systems. This will also bring down area and cost of the hardware components while ensuring power efficient multi-mode operations [1]. Millimeter-wave bands including the 5G-NR (New Radio) bands are projected to be incorporated into 6G systems. While standardization groups have started looking into potential use cases of JC&S (also termed as Integrated Sensing and Communication, i.e. ISAC), the possible hardware solutions are still in early stages of research with physical layer concepts reaching a mature stage. Even though the flexibility of physical layers including waveforms and signal processing algorithms will determine the system requirements, it is clear that an adaptive hardware solution can reduce the added overhead for combining these two functionalities into a single system.

Since there is no guidance for hardware specifications yet for such applications, the first objective towards the realization of JC&S is to understand the effects and performance of combined hardware elements in communication and sensing scenarios beyond a one-size-fits-all approach. In recent years, experimental evaluation of potential JC&S waveforms has been shown in sub-10 GHz and mmWave bands for different applications [2]–[4]. However, standard hardware has been used to conduct these evaluations. In order to co-optimize RF and physical layers, a software-hardware evaluation platform is immediately needed for this topic to proceed further. In this work, a 26 GHz receiver board is developed with reconfigurability functions targeting JC&S applications and evaluated over the air with developed antennas in a Python-based link-level platform. For the design, a communication-centric approach has been adopted compared to a radar-centric approach [5], [6].

Section II gives more details about the receiver architecture while the packaging methodology is described in section III. In section IV, more details about the evaluation setup including the antenna is provided. Section V provides more details about the measurement results. The paper is concluded in section VI.

II. Receiver architecture

The receiver incorporates a 2-stage common-source source-degenerated low noise amplifier (LNA), a Gilbert cell down-conversion mixer and a $50\,\Omega$ output baseband buffer [7]. The receiver blocks are shown in Fig. 1(a). The LNA and mixer are reconfigurable in terms of frequency, gain and linearity. Frequency reconfiguriblity is attained using varactors in the design. The receiver can switch between high gain-low linearity (Mode 1) and low gain-high linearity (Mode 2) modes. Mode 1 comes into play when the signal is severely attenuated whereas, Mode 2 can be made use in the case of close target detection where, the signal at the input of the receiver is much higher. Gain and linearity are made tunable by means of varying the bias voltages of the transistors in the LNA and also the RF transistors in the down-conversion mixer. The chip, as shown in Fig. 1(b) is fabricated in Global Foundries 22 nm FDSOI technology occupying a total area of $0.74\,\mathrm{mm}^2$ including pads. The receiver attains a maximum

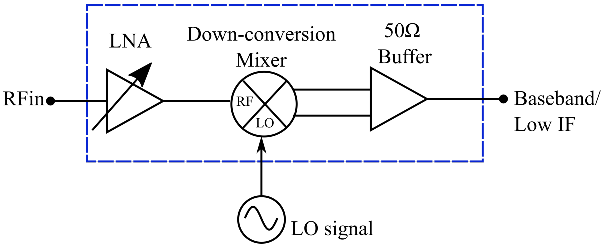

(a)

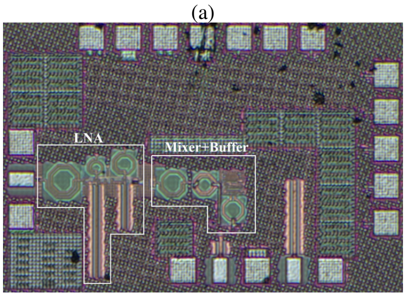

(b)

Fig. 1. (a). Receiver block diagram, (b) Receiver chip micrograph

gain of 22.5 dB at an intermediate frequency (IF) of 400 MHz and a local oscillator (LO) frequency of 25 GHz. The measured input compression point (iP_{1dB}) is at -28 dBm in Mode 1 with a DC power consumption of 22.4 mW. The highest iP_{1dB} achieved in Mode 2 was -20 dBm .

III. PCB Package

Bondwire interconnection is a popular way of chip-to-board interconnection due to its simplicity, fault diagnosing and repeatability in a package design. However, bondwires exhibit a dominant inductive parasitics which becomes a bottleneck with the increasing frequency of operation. Bondwire parasitics depend on loop profile, bonding pad's geometry and operating frequency, that can be estimated through available bondwire models [8]. Therefore, a standard matching network can not be defined and an individual solution needs to be derived for each application. However, a rule of thumb is 0.8-1.0 nH/mm, which can provide a starting point for matching network design.

In this work, the package is designed on RO4003 substrate with 0.508 mm thickness, which is widely available and can be handled in a standard PCB process. The bottom side of the substrate is the ground plane while the chip is bonded on a copper pad on the top side grounded with through hole vias to the bottom grounding. The distance between the chip and bonding pad on PCB is kept at 0.54 mm to enable bonder tool movement during the wire bonding process. 17 µm thick Aluminum wires are used for chip-to-PCB connections using wedge-wedge bonding. Open-stub based parasitic compensation network is applied on RF and LO ports of the package by means of grounded coplanar waveguides (GCPW) that provides a straightforward GSG interface to the chip pads compared to microstrip. The structure is simulated in AWR Analyst EM-Simulator with FEM solver and optimized for input matching as well as insertion loss at RF and LO ports.

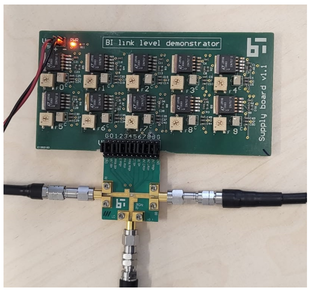

(a)

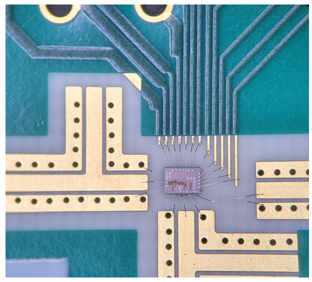

(b)

Fig. 2. (a) LNA-Mixer package with RF, LO and baseband (BB) ports connected to the power supply module (b) Chip to PCB connection with bondwires

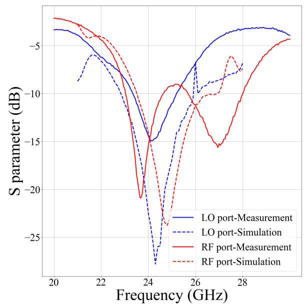

(a)

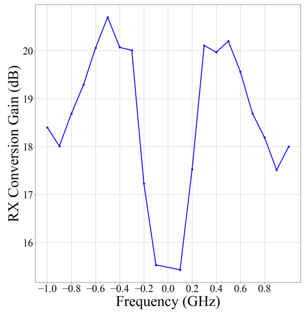

(b)

Fig. 3. (a) RF and LO port matching after wire bonding (b) Modulation frequency characteristic of the receiver package

Ten DC sources are required to power-up the LNA-mixer package with variable voltage setting for tuning and mode configuration of the design. For link-level measurements bulky power supplies are avoided through a customized power supply design based on LT3083 power regulator from Linear Technology. The power supply module can provide 10 independent variable supplies adjustable between 0.1 V to 2.5 V. Each supply output is equipped with a course and fine-tuning control. The DC bias header on the supply module and RF package are provided on the board's edges enabling direct pin-to-pin interface through 2.54 mm pitch jumpers. It minimizes the DC connection length and eliminates the need for additional decoupling capacitors on the package board. The manufactured PCB of the receiver along with the supply board is shown in Fig. 2(a) and a zoom-in is depicted in Fig. 2(b). The S-parameter measurements of the PCB along with the modulation frequency characteristics are shown in Fig. 3(a) and Fig. 3(b) respectively. The minor mismatches are justified because of bondwire loop profile variation between simulation and manufacturing, standard PCB manufacturing tolerance and RPC-2.92 precision connectors (Rosenberger 02K243-40ME3) which provide RF connectivity to the package.

IV. System Setup

In order to evaluate the receiver performance in both sensing and communication applications, it is combined with an external LO, mixer, Power Amplifier (PA), antennas and Universal Software Defined Radio Peripheral (USRP), as depicted in Fig. 4. A constant LO at 25 GHz was fed into the LO port of the up-converter and down-converter mixers. The transmitter side set up was done using an off-the-shelf amplifier (ZVE-323LNX-K+) with $22\,\mathrm{dB}$ gain and a Marki mixer (MM1-2567LS) with a conversion loss of $10\,\mathrm{dB}$ at $26\,\mathrm{GHz}$. The communication receiver measurements were done in a line-of-sight (LOS) scenario with both antennas facing each other. The measurements were done with a pair of horn antennas and patch antennas to understand the system behaviour.

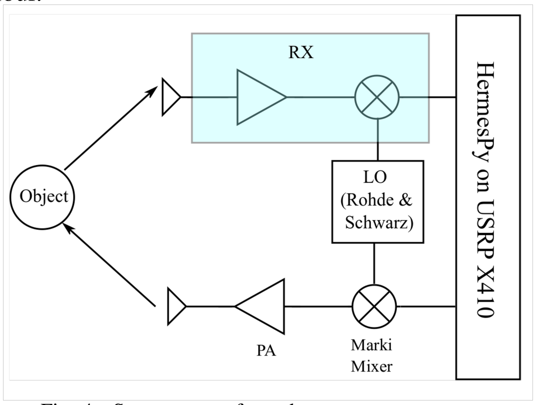

Fig. 4. System setup for radar range measurements

A. Antenna

For the wireless transmission over the air, high gain horn antennas and microstrip patch antennas are employed at the 5G-NR band during the system measurement process. For the horn antennas off-the-shelf linearly polarized wideband high gain antennas, which have an operating frequency range of $4\,\mathrm{GHz}$ to $40\,\mathrm{GHz}$, are chosen. The horn antennas have a gain of on average $13\,\mathrm{dBi}$ in the 5G-NR band and with a half-power beamwidth (HPBW) of 26 degrees in the E-plane. On the other hand, the low-gain patch antennas are designed using a RO4003 substrate with a thickness of $0.508\,\mathrm{mm}$. The snapshot and optimized dimensions of the designed patch antenna are shown in Fig. 5.(a). The simulated and measured reflection coefficients of the patch antenna are shown in Fig. 5.(b). There is very close agreement seen between them indicating that the antenna has a working frequency range from $25.6\,\mathrm{GHz}$ to $26.4\,\mathrm{GHz}$ ($800\,\mathrm{MHz}$). The antenna showed a measured gain of a minimum of $4.78\,\mathrm{dBi}$ and a maximum of $6.1\,\mathrm{dBi}$ in the operating frequency band and the half-power beam width (HPBW) of the antenna is recorded as over 140 degrees in the E-plane. During the system measurements, the antennas are separated by multiple wavelengths to establish isolation between them.

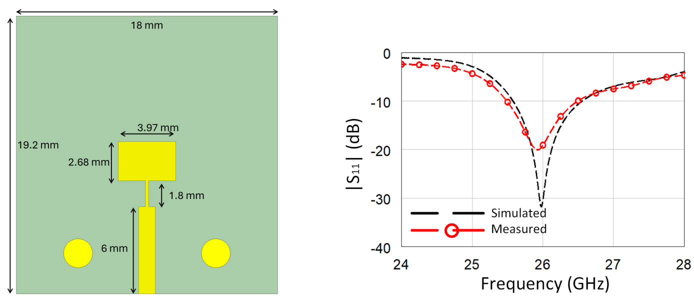

(a) (b)

Fig. 5. (a) Dimensions of the designed patch antenna (b) Simulated and measured reflection coefficient of the patch antenna

B. Software-defined-radio (SDR) and Processing

The USRP is transmitting and receiving waveforms generated and processed by the Heterogeneous Mobile Radio Simulator Python (HermesPy) [9] at $1\,\mathrm{GHz}$ intermediate carrier frequency and $491.52\,\mathrm{MHz}$ sampling rate. The generated waveform is a root-raised cosine single carrier waveform with an effective bandwidth of $245.76\,\mathrm{MHz}$ featuring $128 + 512$ quadrature-amplitude modulated symbols for preamble and data payload, respectively. Considering a monostatic radar illuminating a single target of an unknown radar cross section and neglecting any multipath/clutter effects, the base-band signal reflected by a static target and subsequently sampled by the setup depicted in Fig. 4

$$y(t) = gx\left(t - \frac{2d}{c_0}\right) + n(t) \tag{1}$$

can be expressed depending on the target's distance to the radar d, which causes a signal delay of $2d/c_0$. Here, the speed of light is c_0, additive white Gaussian noise is $n(t) \sim \mathcal{N}(0, \sigma^2)$ of power σ^2, the emitted waveform is $x(t)$ and the channel gain is denoted by g. By correlating the transmitted waveform samples with their received counterparts,

$$P(\hat{d}) = \frac{1}{N-1}\left\|\sum_{l=0}^{N-1} x\left(\frac{l}{f_s}\right) y^*\left(\frac{l+\hat{d}}{f_s}\right)\right\| \tag{2}$$

an estimate of the reflected power depending on the assumed signal delay can be obtained.

V. Measurement Results and Discussions

The results for both microstrip patch and horn antennas and target locations at $1\,\mathrm{m}$ and $1.5\,\mathrm{m}$ distance from the radar transmitter are depicted in Fig. 6(a), (b) and Fig. 6(c), (d) respectively. The maximum value is normalised to a power value of 1 for depiction. It is noted that the setup with horn antennas exhibits a larger detection accuracy. As the distance increases, the performance of the patch antenna degrades. The measurements were also done at $2\,\mathrm{m}$ distance where the patch antennas were not able to detect the target anymore. This indicates that the gain, directivity and bandwidth of the antenna have a clear effect on the object detection and its accuracy.

The performance of the system was also tested in the communication mode. The constellation and eye diagram with horn and patch antennas are shown in Fig. 7 and Fig. 8 respectively. It was noted that the Signal-to-Noise Ratio (SNR) showed a degradation of $6\,\mathrm{dB}$ with patch antennas when compared to the SNR of $42\,\mathrm{dB}$ with horn antennas. This is also reflected in the tighter constellation points when using horn antennas. Note that at the communication receiver, no equalization was performed, which explains the broad constellation points despite the relatively high SNR.

In this work, the receiver and antenna hardware with the software platform have been tested for communication and radar performance parameters. Apart from that, the receiver reconfigurability (from high gain-low linearity to low gain-high linearity modes) has been tested with an isolation-boosted

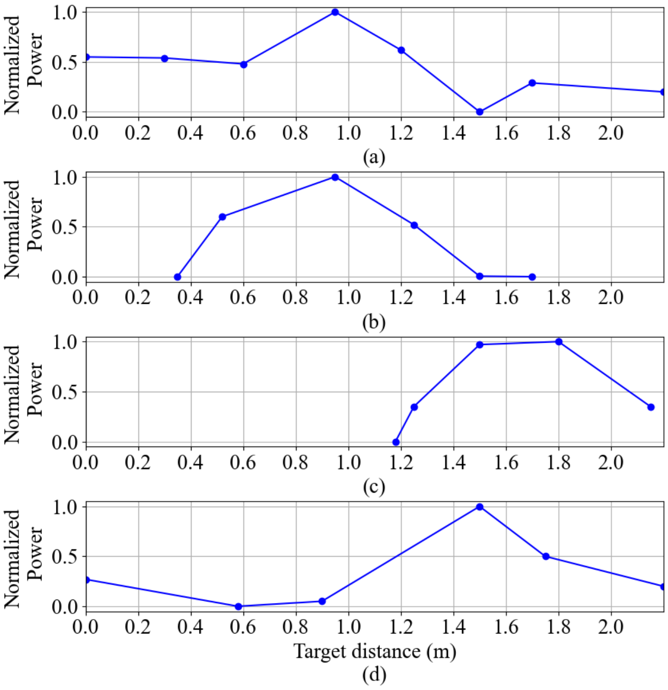

Fig. 6. Range measurements (a) Using patch antenna with object at 1 m (b) Using horn antenna with object at 1 m (c) Using patch antenna with object at 1.5 m (d) Using horn antenna with object at 1.5 m

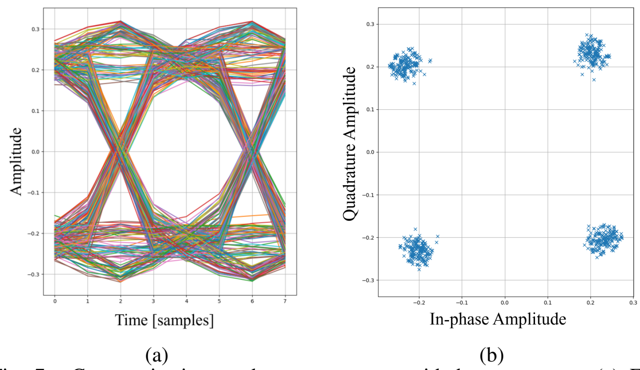

Fig. 7. Communication mode measurements with horn antennas. (a) Eye diagram (b) Constellation

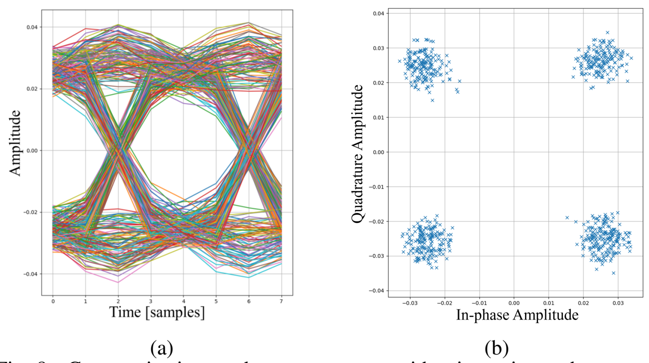

Fig. 8. Communication mode measurements with microstrip patch antennas. (a) Eye diagram (b) Constellation

antenna developed earlier [10]. However, due to the standard transmitter generating double side bands, this could not be tested. As a future work, a wider-bandwidth isolated antenna and a transmitter generating signals in one side band will be used. It was also noted that the isolation between antennas play a crucial role in the system performance. Any leakage due to poor isolation between transmitter and receiver antennas cause the receiver to saturate making the system operation highly non-linear.

VI. Conclusion

The presented work confirms a hardware-software platform that can be used for JC&S transceiver evaluation with standard or custom waveforms and can also be used for bench-marking custom transmitter/receiver architecture. The platform is validated using 5G-NR n258 band. As a future work, we plan to design a high bandwidth high isolation antenna on the same board with the receiver thus utilizing the reconfigurability with a compact form factor. The standard transmitter will also be replaced with a custom JC&S transmitter for benchmarking.

Acknowledgment

This work is financed on the basis of the budget passed by the Saxon State Parliament.

References

[1] S. George, P. Sen, and C. Carta, “Realizing joint communication and sensing rf receiver front-ends: A survey,” *IEEE Access*, vol. 12, pp. 9440–9457, 2024. DOI: 10.1109/ACCESS.2024.3351572.

[2] P. Kumari, S. A. Vorobyov, and R. W. Heath, “Adaptive virtual waveform design for millimeter-wave joint communication–radar,” *IEEE Transactions on Signal Processing*, vol. 68, pp. 715–730, 2020. DOI: 10.1109/TSP.2019.2956689.

[3] S. D. Liyanaarachchi, C. B. Barneto, T. Riihonen, and M. Valkama, “Experimenting joint vehicular communications and sensing with optimized 5g nr waveform,” in *2021 IEEE 93rd Vehicular Technology Conference (VTC2021-Spring)*, 2021, pp. 1–5. DOI: 10 . 1109 / VTC2021-Spring51267.2021.9448834.

[4] T. M. Pham, R. Bomfin, A. Nimr, A. N. Barreto, P. Sen, and G. Fettweis, “Joint communications and sensing experiments using mmwave platforms,” in *2021 IEEE 22nd International Workshop on Signal Processing Advances in Wireless Communications (SPAWC)*, 2021, pp. 501–505. DOI: 10.1109/SPAWC51858.2021.9593174.

[5] N. Souzandeh, M. Harifi-Mood, J. Pourahmadazar, S. Aïssa, and S. O. Tatu, “Mm-wave joint sensing and communication system,” in *2023 20th European Radar Conference (EuRAD)*, 2023, pp. 274–277. DOI: 10.23919/EuRAD58043.2023.10289489.

[6] S. Şahin and T. Girici, “A novel radar receiver for joint radar and communication systems,” in *2023 International Conference on Radar, Antenna, Microwave, Electronics, and Telecommunications (ICRAMET)*, 2023, pp. 61–66. DOI: 10.1109/ICRAMET60171.2023.10366608.

[7] S. George, P. Sen, and C. Carta, “A multi-mode direct conversion receiver for joint communication and radar sensing,” in *2024 15th German Microwave Conference (GeMiC)*, 2024, pp. 229–232. DOI: 10.23919/GeMiC59120.2024.10485239.

[8] M. Umar, M. Laabs, N. Neumann, and D. Plettemeier, “Bondwire model and compensation network for 60 ghz chip-to-pcb interconnects,” *IEEE Antennas and Wireless Propagation Letters*, vol. 20, no. 11, pp. 2196–2200, 2021. DOI: 10.1109/LAWP.2021.3108499.

[9] J. Adler, T. Kronauer, and A. N. Barreto, “Hermespy: An open-source link-level evaluator for 6g,” *IEEE Access*, vol. 10, pp. 120 256–120 273, 2022. DOI: 10.1109/ACCESS.2022.3222063.

[10] M. Ramzan, A. N. Barreto, and P. Sen, “Meta-surface boosted antenna to achieve higher than 50 db trx isolation at 26 ghz for joint communication and radar sensing (jcs),” in *2022 16th European Conference on Antennas and Propagation (EuCAP)*, 2022, pp. 1–5. DOI: 10.23919/EuCAP53622.2022.9769327.